Research Letter **DOI:** 10.15541/jim20240202

In-situ Growth of Conformal SnO_2 Layers for Efficient Perovskite Solar Cells

LIU Suolan[1,2], LUAN Fuyuan[1,3], WU Zihua[3,4], SHOU Chunhui[5], XIE Huaqing[3,4], YANG Songwang[1,2]

(1. CAS Key Laboratory of Materials for Energy Conversion, Shanghai Institute of Ceramics, Chinese Academy of Sciences, Shanghai 201899, China; 2. Center of Materials Science and Optoelectronics Engineering, University of Chinese Academy of Sciences, Beijing 100049, China; 3. School of Energy and Materials, Shanghai Polytechnic University, Shanghai 201209, China; 4. Shanghai Engineering Research Center of Advanced Thermal Functional Materials, Shanghai 201209, China; 5. Zhejiang Baima Lake Laboratory Co. Ltd., Hangzhou 310000, China)

Abstract: Significant progress has recently been made in enhancing the power conversion efficiency (PCE) of perovskite solar cells (PSCs). The electron transport layer (ETL), as an essential component of PSCs, significantly influences the performance of devices. Traditional spin-coating method for preparing the ETL fails to fully cover the cusp of FTO transparent conductive glass substrate, leading to direct contact between perovskite film and FTO substrate, which induces charge recombination and reduces the performance of PSCs. To address this issue, an *in-situ* growth method was proposed to prepare conformal SnO_2 films on FTO glass substrates in this study. The resulting SnO_2 films are not only dense and uniform, fully covering the cusp of the FTO glass substrates and reducing the contact area between the FTO substrates and the perovskite films, but also facilitating the formation of perovskite films with large grain sizes. Moreover, the conformal SnO_2 films can improve the charge extraction at the SnO_2/perovskite interface, reduce the trap density and trap-assisted recombination in PSCs, and thus enhance the PCE of PSCs. Through comparative experiments, it is found that the PSCs with *in-situ* grown SnO_2 films show an improved PCE of 21.97%, which significantly increased compared to that with spin-coated SnO_2 films (20.93%). All above data demonstrate that the as-prepared SnO_2 film can serve as an ideal ETL. It is worth mentioning that this method avoids the use of corrosive hydrochloric acid and toxic thioglycolic acid, and it can also be extended to ITO flexible transparent conductive substrates in the future.

Key words: perovskite solar cell; conformal SnO_2 film; *in-situ* growth

Perovskite solar cells have garnered significant attention from research communities over the past decade, with the power conversion efficiency (PCE) increasing from 3.8% to 26.1%[1-4]. It is anticipated that the PSCs are expected to develop as one of the third-generation solar cells in the future[5]. Apart from optimizing the perovskite absorber layer, it is imperative to prepare an effective electron transport material that affects the charge extraction and transport at the interface[6-10].

In the early stages of research on PSCs, most researchers used titanium dioxide (TiO_2) as the electron transport layer (ETL), which typically requires a high sintering temperature (>450 ℃) after spin-coating[11-13]. In addition, TiO_2 was found to have vigorous photocatalytic activity under ultraviolet light, inducing the decomposition of perovskite films, thereby hindering device stability and commercial application. In contrast, SnO_2 has better chemical stability, higher light transmittance and greater electron mobility[14-16]. Furthermore, the conduction band minimum of SnO_2 is conducive to electron extraction due to its proximity to the bottom of the conduction band of the perovskite[17-19]. Currently, spin-coating SnO_2 colloidal solution is commonly used to prepare SnO_2 films[20-22], but it yields nonuniform coverage on the rough FTO glass substrates. Chemical bath deposition (CBD) has attracted notable attention as an ideal method for preparing SnO_2 ETL under low-temperature conditions[23-24]. For instance, a three-step CBD method was proposed to utilize SnO_2/TiO_2 as the ETL to enhance electron extraction and

Received date: 2024-04-18; **Revised date:** 2024-06-20; **Published online:** 2024-07-16
Foundation item: Space Application System of China Manned Space Program
Biography: LIU Suolan (1999–), female, Master candidate. E-mail: liusuolan21@mails.ucas.ac.cn
刘锁兰(1999–), 女, 硕士研究生. E-mail: liusuolan21@mails.ucas.ac.cn
Corresponding author: YANG Songwang, professor. E-mail: swyang@mail.sic.ac.cn
杨松旺, 研究员. E-mail: swyang@mail.sic.ac.cn

suppress carrier recombination at the SnO_2/perovskite interface[25]. A low concentration of $SnCl_2$•$2H_2O$ solution was used to repeat the CBD method three times to obtain a uniform ETL[26]. Nevertheless, the CBD method relies on corrosive hydrochloric acid and toxic thioglycolic acid to prevent particle aggregation in the precursor solution, posing potential environmental pollution concerns. Hence, it is necessary to develop an environmentally friendly and facile method to prepare uniform and well-covered SnO_2 films on the FTO glass substrates.

In this work, a low-temperature, environmentally friendly, and *in-situ* growth (IG) method was employed to prepare a dense and uniform SnO_2 ETL. The IG SnO_2 film facilitates charge extraction at the buried interface and promotes the formation of large-sized perovskite grains, which holds great promise in achieving high-performance PSCs.

1 Experimental

1.1 Materials

Dimethylsulfoxide (DMSO, 99.99%), acetonitrile (ACN, 99.8%), *N*, *N*-dimethylformamide (DMF, 99.8%), chlorobenzene (CB, 99.99%), 4-tert-butylpyridine (TBP, 98%) and bis(trifluoromethylsulfonyl)-imide lithium salt (LiTFSI, 99.9%) were purchased from Sigma-Aldrich. Phenethylammonium iodide (PEAI, 99.5%) and lead iodide (PbI_2, 99.99%) were purchased from Xi'an Yuri Solar. Methylammonium iodide (MAI, 99.9%) and formamidinium iodide (FAI, 99.9%) were purchased from Greatcell Solar Materials. $SnCl_4$•$5H_2O$ (99.998%) was purchased from Macklin. Molybdenum trioxide (MoO_3, 99.95%) and methylammonium chloride (MACl, 98%) were purchased from Aladdin. Isopropanol (IPA, 99.9%) and tin (IV) oxide (SnO_2, 15% colloidal water dispersion) were purchased from Alfa Aesar. Fluorine-doped tin oxide (FTO, 14 Ω) glass was purchased from AGC. FK209 (Co(III) TFSI salt, 99%) and 2,2′,7,7′-tetrakis(*N*,*N*-*p*-dimethoxy-phenylamino)-9,9′-spirobifluorene (Spiro-OMeTAD, 99.8%) were purchased from Lumtec. All chemicals were used without further purification.

1.2 Growth of SnO_2 films

The FTO glass substrates were washed ultrasonically with aqueous detergent solution, deionized water, acetone, and ethanol for 6 h in sequence. Then, they were dried with an air gun. A commercial SnO_2 colloidal dispersion (Alfa Aesar) was spin-coated to prepare spin-coated SnO_2 (SC SnO_2) films. The SnO_2 colloidal solution was dissolved in deionized water at the volume ratio of 1∶3 to prepare the SnO_2 precursor solution. Before spin-coating, the SnO_2 precursor solution and the FTO glass substrates were treated by a UV-Ozone cleaner for 15 min to remove residual organics. Subsequently, 100 μL of the SnO_2 precursor solution was dropped on the FTO glass substrates and spin-coated at 4000 r/min for 30 s. Then, the substrates were placed on a 150 ℃ hot plate for 30 min to afford the SC SnO_2 films.

IG SnO_2 films were prepared through an *in-situ* growth method. Firstly, 600 mg of $SnCl_4$•$5H_2O$ was dissolved in 15 mL of deionized water and stirred for 10 min, and then 15 mL of water was added to the bottom of a hydrothermal reaction vessel, with a petri dish positioned atop a bracket. The FTO glass substrates were immersed in 15 mL of $SnCl_4$•$5H_2O$ aqueous solution in the petri dish. Then, the hydrothermal reactor was placed in a 120 ℃ oven for 20 h. After the reactor cooled down, the FTO/SnO_2 films were put into deionized water and ethanol with ultrasonic treatment for 1 h, respectively. Following this treatment, the obtained dense SnO_2 layers on the FTO glass substrates were dried by an air gun without further annealing treatment.

1.3 Preparation of precursor solution

PbI_2 precursor solution: 692 mg of PbI_2 was dissolved in the mixed solvent of 900 μL of DMF and 100 μL of DMSO and then placed on a 70 ℃ hot plate for 4 h, and filtered through a 0.45 μm filter before use.

Organic ammonium salt precursor solution: 9 mg of MACl, 90 mg of FAI, and 6.4 mg of MAI were dissolved in 1 mL of IPA and stirred overnight. PEAI precursor solution: 5 mg of PEAI was dissolved in 1 mL of IPA and stirred overnight.

Spiro-OMeTAD precursor solution: Spiro-OMeTAD (72.3 mg) was dissolved in 1 mL of CB. Then, 28.8 μL of TBP and 17.5 μL of LiTFSI solution (0.52 g of LiTFSI dissolved in 1 mL of ACN) were added. Subsequently, 29 μL of FK209 solution (0.30 g of FK209 dissolved in 1 mL of ACN) was added to oxidize Spiro-OMeTAD. The solution was stirred overnight and filtered through a 0.45 μm filter before use.

1.4 Fabrication of perovskite solar cells

The FTO glass substrates were treated with a UV-Ozone cleaner for 15 min to enhance their wettability with the PbI_2 solution. They were then transferred into a dry-air glove box (relative humidity<15%) to spin-coat each functional layer. A two-step method was used to fabricate the photoactive perovskite layer. The PbI_2 precursor solution was preheated on a 70 ℃ hot plate for 10 min, and then 70 μL of that was spin-coated on the SnO_2 layer at 2000 r/min for 30 s. Then, the PbI_2 film was placed on a hot plate at 70 ℃ for 1 min. After the PbI_2 film cooled down, it was spin-coated with an organic ammonium salt solution. The spin-coating speed of the organic ammonium salt solution was the same as

that of the PbI_2 solution. After that, the wet perovskite film was immediately transferred to a 150 ℃ hot plate for 15 min to evaporate the IPA solvent. After the perovskite film cooled to room temperature, 120 μL of PEAI precursor solution was spin-coated on the perovskite films at 3000 r/min for 30 s by dynamic spin-coating, followed by 15 min of vacuuming treatment. Next, 30 μL of Spiro-OMeTAD precursor solution was spin-coated on the PEAI passivation layer at 4000 r/min for 30 s. Finally, 7.5 nm MoO_3 and 100 nm Ag were prepared by thermal evaporation to afford the PSCs with the structure of FTO/SnO_2/$FA_{0.92}MA_{0.08}PbI_3$/PEAI/Spiro-OMeTAD/MoO_3/Ag.

2　Results and discussion

Fig. 1(a) shows the top-view scanning electron microscopy (SEM) image of FTO glass substrate for reference. As shown in Fig. 1(b-e), the cusp of the FTO glass substrate was not fully covered by SC SnO_2 film, while IG SnO_2 film completely covered the cusp of the FTO glass substrate. The IG SnO_2 film with a smaller particle size and a thickness of ~20 nm, thinner than the SC SnO_2 film (30 nm), is less prone to aggregation on the FTO glass substrate. Fig. 1(f) shows the transmittance spectra of SC SnO_2, IG SnO_2 film and FTO glass substrate. The transmittance of IG SnO_2 film is higher than that of SC SnO_2 film, particularly ranging from 300 to 700 nm. This is attributed to the anti-reflection property of IG SnO_2, facilitating more efficient light absorption of perovskite film. From the atomic force microscopy (AFM) measurements, the average roughness (R_a) of FTO glass substrate, SC SnO_2 film, and IG SnO_2 film is 26.43, 28.20, and 32.89 nm, respectively, as shown in Fig. 1(g-i). The conformal and uniform coverage of IG SnO_2 films on the FTO glass substrates reduces the carrier combination centers that arise from the direct contact between FTO and perovskite.

The $FA_{0.92}MA_{0.08}PbI_3$ perovskite film was prepared on the SnO_2 film by a two-step spin-coating method. The cross-sectional SEM images (Fig. 2(a, b)) show that the perovskite film obtained on the IG SnO_2 film has more regular columnar grains compared to the SC SnO_2 film. As shown in Fig. 2(c), the steady-state photoluminescence (PL) spectrum of the perovskite film deposited on the IG SnO_2 film shows a weaker PL intensity, which suggests that the photogenerated electrons can be extracted more efficiently at the IG SnO_2/perovskite interface. This kind of morphology promotes effective charge extraction and

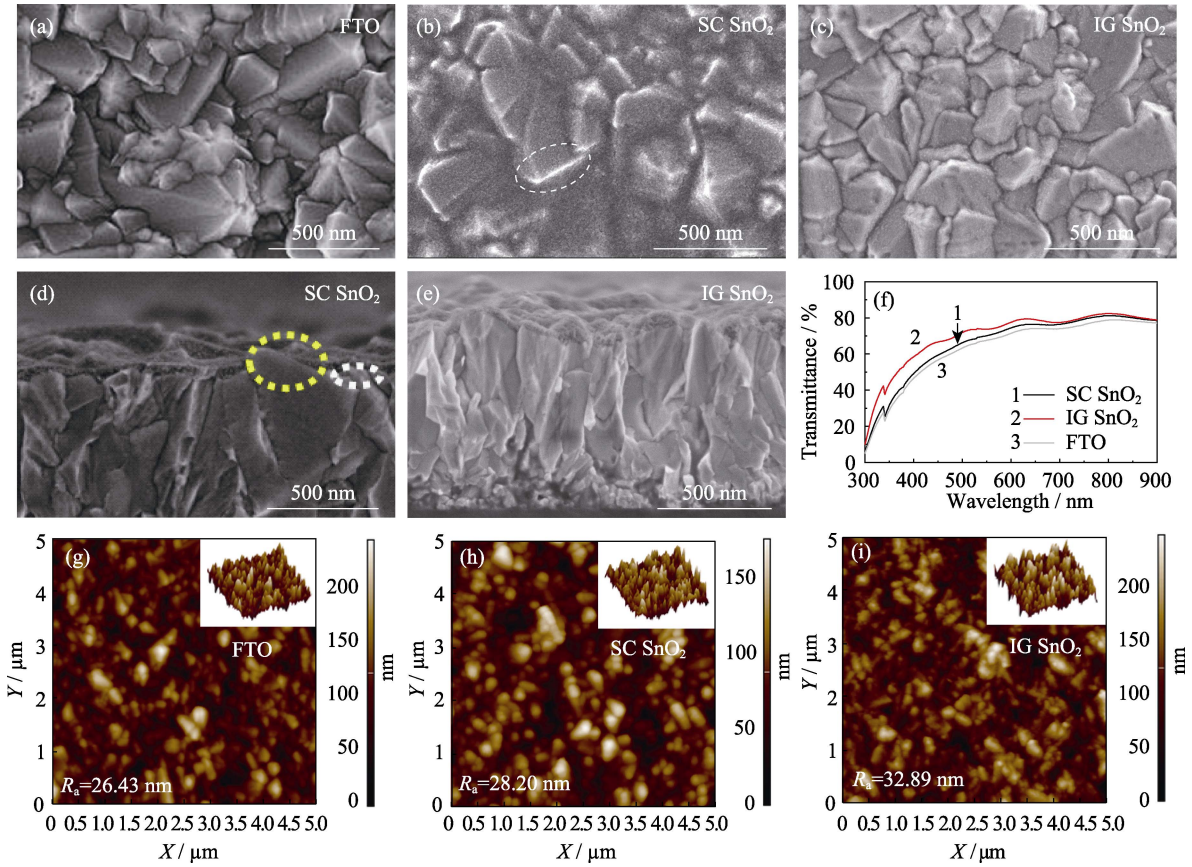

Fig. 1　SEM, AFM morphologies, and transmittance of FTO glass substrate, SC SnO_2 and IG SnO_2 films

(a-c) Top-view SEM images of (a) FTO glass substrate, (b) SC SnO_2 and (c) IG SnO_2 films; (d, e) Cross-sectional SEM images of (d) SC SnO_2 and (e) IG SnO_2 films; (f) Transmittance spectra of SC SnO_2, IG SnO_2 films and FTO glass substrate; (g-i) AFM images of (g) FTO glass substrate, (h) SC SnO_2 and (i) IG SnO_2 films with insets showing the corresponding 3D images

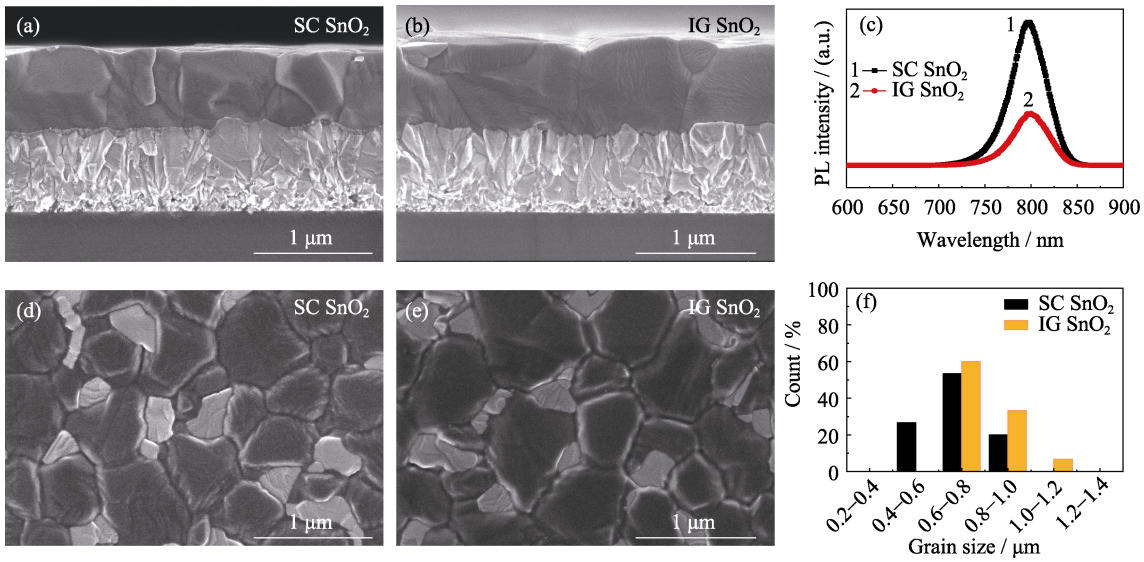

Fig. 2 SEM morphologies, photoluminescence properties, and grain size distributions of perovskite films

(a, b) Cross-sectional SEM images of perovskite films deposited on (a) SC SnO_2 and (b) IG SnO_2 films; (c) Steady-state PL spectra of perovskite films deposited on SC SnO_2 and IG SnO_2 films; (d, e) Top-view SEM images of perovskite films deposited on (d) SC SnO_2 and (e) IG SnO_2 films; (f) Grain size distribution histograms of perovskite films corresponding to (d, e)

transport[27]. The top-view SEM images of the perovskite surface are shown in Fig. 2(d, e). The grains of the perovskite film on the IG SnO_2 film are larger than those on the SC SnO_2 film. Based on the SC SnO_2 film, as shown in Fig. 2(f), the average grain size of the perovskite film is 700 nm (accounting for 53.4%), while on the IG SnO_2 film, the average grain size increases to 800 nm (accounting for 60.0%). This indicates that IG SnO_2 is beneficial for the formation of high-quality perovskite films.

To investigate the influence of IG SnO_2 on device performance, SC SnO_2 and IG SnO_2 films were used as electron transport layers to fabricate n-i-p structure PSCs. Fig. 3(a) shows *J*–*V* curves of PSCs with different SnO_2 films. It is evident that IG SnO_2 device exhibits higher open-circuit voltage (V_{OC}) and fill factor (FF) than SC SnO_2 device, which is attributed to the reduction of recombination centers at the buried interface. The IG SnO_2 device shows the highest PCE (21.97%) with short-circuit current density (J_{SC}) of 25.14 mA·cm^{-2}, V_{OC} of 1.131 V and FF of 77.25%. In contrast, the SC SnO_2 device exhibits a lower PCE of 20.93%, with J_{SC} of 24.81 mA·cm^{-2}, V_{OC} of 1.110 V and FF of 76.04%. Table S1 presents the statistical data of twenty individual devices fabricated with SnO_2 films by spin-coating and *in-situ* growth method. Compared to those of SC SnO_2 devices, IG SnO_2 devices show improvements in photovoltaic parameters. The average V_{OC} increases from 1.095 V to 1.117 V, the average J_{SC} increases from 24.91 mA·cm^{-2} to 25.06 mA·cm^{-2}, the average FF increases from 73.65% to 76.65%, and the average PCE increases from 20.08% to 21.45%. The incident photon-to-electron conversion efficiency (IPCE) spectra are shown in Fig. 3(b), and the integrated current density ($J_{SC,\ IPCE}$) of the SC SnO_2 device is 23.88 mA·cm^{-2}, while that of the IG SnO_2 device increases to 24.53 mA·cm^{-2} due to the anti-reflection property of the IG SnO_2 layer. As shown in Fig. 3(c-f), V_{OC}, J_{SC}, FF and PCE distributions of the SC SnO_2 and IG SnO_2 devices were tested under a standard solar simulator (AM 1.5 G, 100 mW·cm^{-2}). V_{OC}, FF, and J_{SC} of the IG SnO_2 devices were enhanced, resulting in an increment of PCE. Transient photocurrent (TPC) and transient photovoltage (TPV) measurements were conducted to investigate the photogenerated electron extraction and transfer. The exponential function was used to fit the TPV and TPC decay curves, and the function used is shown as follows:

$$y = y_0 + \sum A_i \exp\left(\frac{t}{\tau_i}\right) \quad (1)$$

Where τ represents carrier lifetime of perovskite film (μs) and A is amplitude coefficient. The calculation formula of the average carrier lifetime τ_{avg} is given as follows:

$$\tau_{avg} = \frac{\sum A_i \tau_i^2}{\sum A_i \tau_i} \quad (2)$$

The carrier lifetime τ, derived from the TPC decay curves (using a single exponential function), decreases from 7.45 μs to 4.23 μs (Fig. 3(g) and Table S2). This implies that IG SnO_2 enhances charge extraction, indicating a faster transfer rate of carriers from the perovskite layer to the SnO_2 layer. Table S2 presents the carrier lifetime τ obtained by fitting the TPV decay

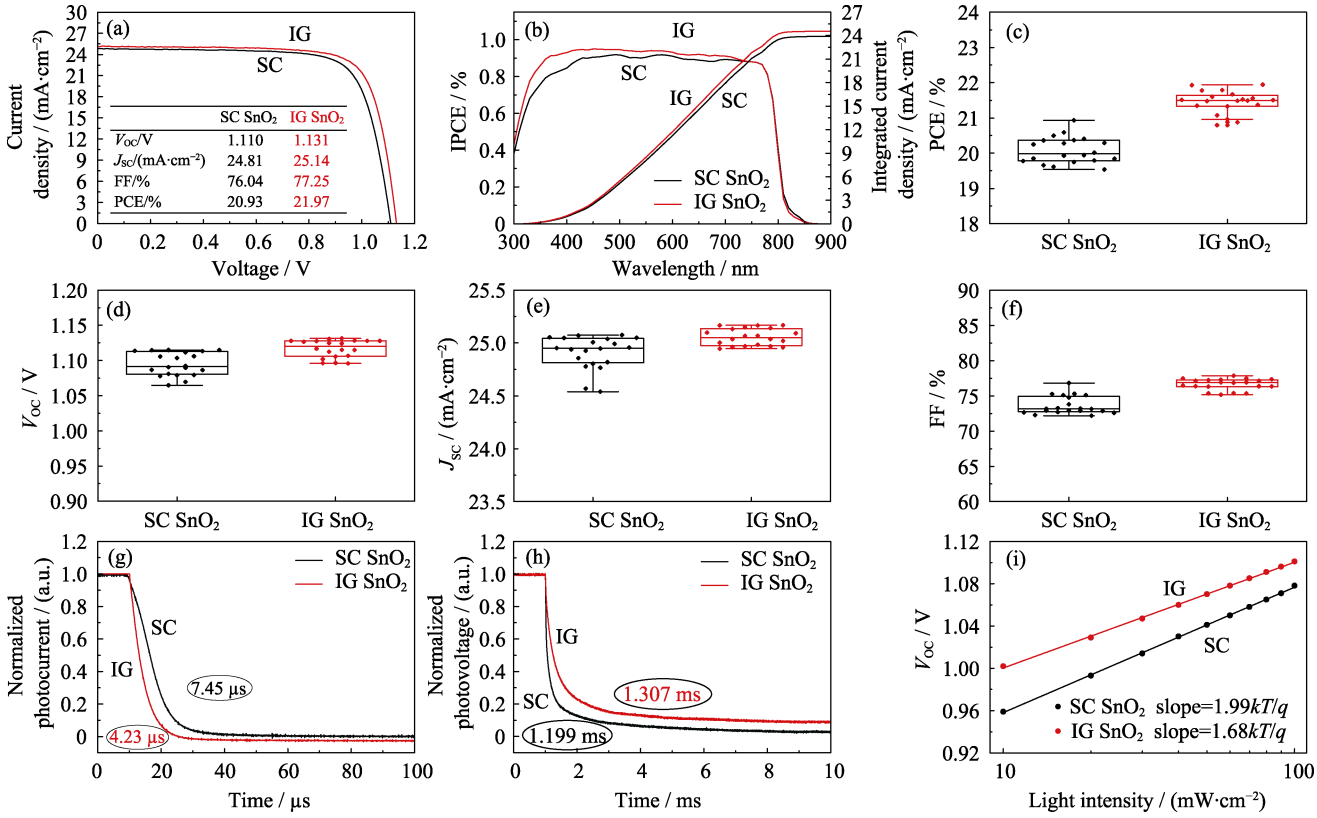

Fig. 3　Photovoltaic performance of PSCs based on SC SnO_2 and IG SnO_2 films

(a) *J*–*V* curves; (b) IPCE spectra; (c-f) Statistical distributions of (c) PCE, (d) V_{OC}, (e) J_{SC}, and (f) FF; (g) TPC decay curves; (h) TPV decay curves; (i) V_{OC} dependent curves of the light intensity

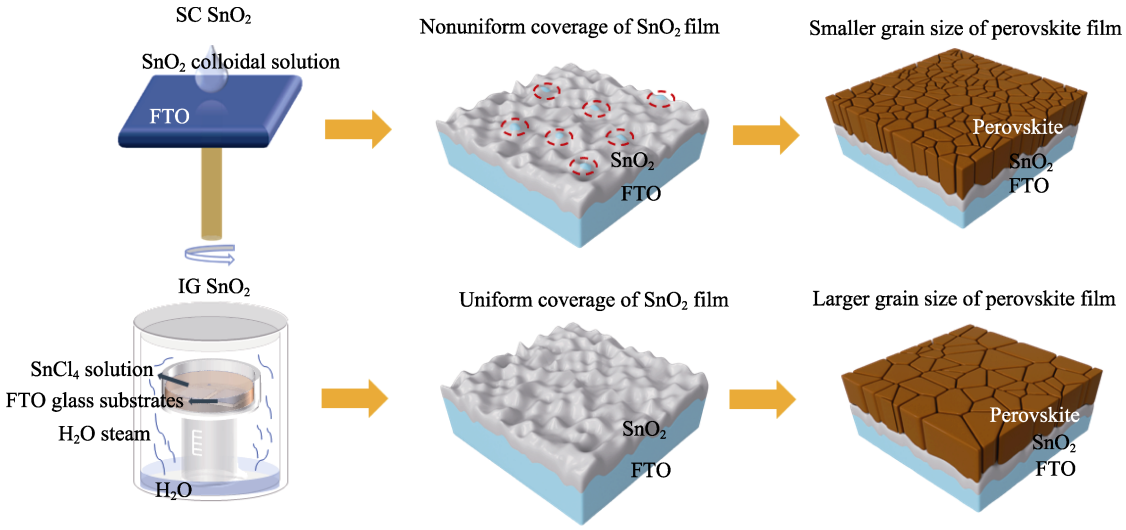

Fig. 4　Schematic illustration of the growth of SnO_2 and perovskite layer

curves using biexponential functions, which displays two distinct electron lifetimes: one characterized by fast decay component τ_1 attributed to electron transport and another characterized by slow decay component τ_2 associated with trap depopulation kinetics. The prolonged τ_{avg} observed in the IG SnO_2 device (Fig. 3(h)) suggests a decrease of trap density and significant suppression of carrier recombination (1.199 ms for the SC SnO_2 device and 1.307 ms for the IG SnO_2 device)[28]. Generally, a short carrier recombination lifetime of perovskite film and a fast carrier transfer rate at the buried interface ensure the efficient utilization of the carriers.

Fig. 3(i) shows the V_{OC} dependence of the light intensity with a slope equal to nkT/q, where n (ideal factor) reflects the degree of trap-assisted recombination, k is the Boltzmann constant (1.38×10^{-23} J·K^{-1}), T is the thermodynamic temperature (K) and q is the elementary charge (1.60×10^{-19} C). When n is close to 2, trap-assisted

recombination (Shockley-Read-Hall) dominates[29]. The slopes of SC SnO_2 device and IG SnO_2 device are $1.99kT/q$ and $1.68kT/q$, respectively. n of the IG SnO_2 device is smaller than that of the SC SnO_2 device, which indicates that its trap-assisted recombination is reduced.

Based on the above analysis, a possible mechanism for perovskite layer fabrication on SC SnO_2 and IG SnO_2 films is proposed (Fig. 4). When the spin-coating method is used to prepare SnO_2 films, the rough surface of the FTO glass substrates with an undulation of approximately 200 nm leads to an incomplete coverage and nonuniform thickness of the SnO_2 layers. However, the *in-situ* growth method not only enables the uniform coverage of SnO_2 films on the FTO glass substrates, but also helps to form large-sized perovskite grains.

3 Conclusions

In this study, a simple and environmentally friendly *in-situ* growth method for preparing a conformal SnO_2 ETL was developed. The perovskite films grown on this kind of SnO_2 layer exhibit large grain sizes. Furthermore, the IG SnO_2 films facilitate charge extraction at the buried interface and suppress trap-assisted recombination of perovskite film. Consequently, PSCs fabricated with IG SnO_2 films achieved an enhanced PCE of 21.97%, compared to 20.93% of PSCs with SC SnO_2 films. Furthermore, as the *in-situ* growth method is acid-free and avoids corrosion of the ITO substrates, this method can be extended to flexible PSCs.

Supporting Materials

Supporting materials related to this article can be found at https://doi.org/10.15541/jim20240202.

References:

[1] HUANG Z, BAI Y, HUANG X, *et al.* Anion–π interactions suppress phase impurities in $FAPbI_3$ solar cells. *Nature*, 2023, **623(7987):** 531.

[2] KOJIMA A, TESHIMA K, SHIRAI Y, *et al.* Organometal halide perovskites as visible-light sensitizers for photovoltaic cells. *J. Am. Chem. Soc.*, 2009, **131(17):** 6050.

[3] PARK J, KIM J, YUN H S, *et al.* Controlled growth of perovskite layers with volatile alkylammonium chlorides. *Nature*, 2023, **616(7958):** 724.

[4] LIANG Z, ZHANG Y, XU H, *et al.* Homogenizing out-of-plane cation composition in perovskite solar cells. *Nature*, 2023, **624(7992):** 557.

[5] WANG R, MUJAHID M, DUAN Y, *et al.* A review of perovskites solar cell stability. *Adv. Funct. Mater.*, 2019, **29(47):** 1808843.

[6] HUI W, KANG X, WANG B, *et al.* Stable electron-transport-layer-free perovskite solar cells with over 22% power conversion efficiency. *Nano Lett.*, 2023, **23(6):** 2195.

[7] LIU Q, LIU Y, LIU H, *et al.* Magnetron sputtering Zn_2SnO_4 electron-transport layer for all room-temperature-processed perovskite solar cells. *Sol. RRL*, 2024, **8(4):** 2300926.

[8] KIMATA H, YAMAGUCHI S, GOTANDA T, *et al.* Open-circuit-voltage improvement mechanism of perovskite solar cells revealed by operando spin observation. *ACS Appl. Mater. Interfaces*, 2023, **15(50):** 58539.

[9] GOU Y, WANG H, LI Y, *et al.* Developing a gradient titanium dioxide/amorphous tantalum nitride electron transporting layer for efficient and stable perovskite solar cells. *Inorg. Chem. Front.*, 2023, **10(22):** 6622.

[10] LIU J, YIN Y, HE B, *et al.* Focusing on the bottom contact: carbon quantum dots embedded SnO_2 electron transport layer for high-performance and stable perovskite solar cells. *Mat. Today Phys.*, 2023, **33:** 101041.

[11] HU W, ZHOU W, LEI X, *et al.* Low-temperature *in situ* amino functionalization of TiO_2 nanoparticles sharpens electron management achieving over 21% efficient planar perovskite solar cells. *Adv. Mater.*, 2019, **31(8):** 1806095.

[12] JIANG Z, HE Z, MA S, *et al.* Effect of yttrium-incorporated TiO_2 electron transport layer on the photovoltaic performance of triple-cation perovskite solar cells. *J. Phys. Chem. C*, 2023, **127(39):** 19432.

[13] HE J, DING T, WU W. Surface lattice perturbation of electron transport layer reducing oxygen vacancies for positive photovoltaic effect. *Sol. RRL*, 2022, **6(10):** 2200226.

[14] LI S, YANG Y, SU K, *et al.* Dopant-free small molecule hole transport materials based on triphenylamine derivatives for perovskite solar cells. *Chin. J. Chem. Eng.*, 2022, **50:** 29.

[15] YOU S, ZENG H, KU Z, *et al.* Multifunctional polymer-regulated SnO_2 nanocrystals enhance interface contact for efficient and stable planar perovskite solar cells. *Adv. Mater.*, 2020, **32(43):** 2003990.

[16] LIN L, JONES T W, YANG T C J, *et al.* Inorganic electron transport materials in perovskite solar cells. *Adv. Funct. Mater.*, 2021, **31(5):** 2008300.

[17] BU T, LI J, ZHENG F, *et al.* Universal passivation strategy to slot-die printed SnO_2 for hysteresis-free efficient flexible perovskite solar module. *Nat. Commun.*, 2018, **9(1):** 4609.

[18] LEE H B, JEON M K, KUMAR N, *et al.* Boosting the efficiency of SnO_2-triple cation perovskite system beyond 20% using nonhalogenated antisolvent. *Adv. Funct. Mater.*, 2019, **29(32):** 1903213.

[19] MÉNDEZ P F, MUHAMMED S K M, BAREA E M, *et al.* Analysis of the UV–Ozone-treated SnO_2 electron transporting layer in planar perovskite solar cells for high performance and reduced hysteresis. *Sol. RRL*, 2019, **3(9):** 1900191.

[20] ZHOU J, ZHOU R, ZHU J, *et al.* Colloidal SnO_2-assisted CdS electron transport layer enables efficient electron extraction for planar perovskite solar cells. *Sol. RRL*, 2021, **5(9):** 2100494.

[21] LIU H, CHEN Z, WANG H, *et al.* A facile room temperature solution synthesis of SnO_2 quantum dots for perovskite solar cells. *J. Mater. Chem. A*, 2019, **7(17):** 10636.

[22] SONG K K, ZOU X P, ZHANG H Y, *et al.* Effect of SnO_2 colloidal dispersion solution concentration on the quality of perovskite layer of solar cells. *Coatings*, 2021, **11(5):** 591.

[23] CORREA BAENA J P, STEIER L, TRESS W, *et al.* Highly efficient planar perovskite solar cells through band alignment engineering. *Energy Environ. Sci.*, 2015, **8(10):** 2928.

[24] ANARAKI E H, KERMANPUR A, MAYER M T, *et al.* Low-temperature Nb-doped SnO_2 electron-selective contact yields over 20% efficiency in planar perovskite solar cells. *ACS Energy Lett.*, 2018, **3(4):** 773.

[25] DING B, HUANG S Y, CHU Q Q, *et al.* Low-temperature SnO_2-modified TiO_2 yields record efficiency for normal planar perovskite solar modules. *J. Mater. Chem. A*, 2018, **6(22):** 10233.

[26] BU T, LIU X, ZHOU Y, *et al.* A novel quadruple-cation absorber for universal hysteresis elimination for high efficiency and stable perovskite solar cells. *Energy Environ. Sci.*, 2017, **10(12):** 2509.
[27] WU C, FANG W, CHENG Q, *et al.* MXene-regulated perovskite vertical growth for high-performance solar cells. *Angew. Chem. Int. Ed.*, 2022, **61(43):** e202210970.
[28] ZOU Y, EICHHORN J, RIEGER S, *et al.* Ionic liquids tailoring crystal orientation and electronic properties for stable perovskite solar cells. *Nano Energy*, 2023, **112:** 108449.
[29] DOU J, ZHU C, WANG H, *et al.* Synergistic effects of Eu-MOF on perovskite solar cells with improved stability. *Adv. Mater.*, 2021, **33(39):** 2102947.

原位生长钙钛矿太阳能电池共形氧化锡薄膜

刘锁兰[1,2], 栾福园[1,3], 吴子华[3,4], 寿春晖[5], 谢华清[3,4], 杨松旺[1,2]

(1. 中国科学院 上海硅酸盐研究所, 中国科学院能量转换材料重点实验室, 上海 201899; 2. 中国科学院大学 材料科学与光电工程中心, 北京 100049; 3. 上海第二工业大学 能源与材料学院, 上海 201209; 4. 上海先进热功能材料工程技术研究中心, 上海 201209; 5. 浙江省白马湖实验室有限公司, 杭州 310000)

摘 要: 近年来, 钙钛矿太阳能电池(PSCs)的光电转换效率(PCE)取得了重要进展, 其中, 电子传输层作为重要组成部分, 对 PSCs 的性能有显著影响。传统旋涂法制备的电子传输层(ETL)难以完全覆盖 FTO 透明导电衬底尖端, 使得钙钛矿薄膜与 FTO 衬底直接接触, 导致电荷复合, PSCs 性能降低。针对这一问题, 本研究提出了一种原位生长方法, 在 FTO 玻璃衬底上制备共形的 SnO_2 薄膜。所得 SnO_2 薄膜不仅致密均匀, 而且能够覆盖 FTO 玻璃衬底尖端, 降低 FTO 衬底与钙钛矿薄膜的接触面积, 使在其上制备的钙钛矿薄膜具有更大的晶粒尺寸。此外, 共形的 SnO_2 薄膜还能促进 SnO_2/钙钛矿界面电荷的有效提取, 降低 PSCs 的陷阱密度, 抑制陷阱辅助的电荷复合, 从而提升 PSCs 的 PCE。对比实验发现, 当 PSCs 采用原位生长 SnO_2 薄膜时, 其 PCE 提升至 21.97%, 相较于采用旋涂法制备的 SnO_2 薄膜(20.93%)有了明显提升, 表明原位生长 SnO_2 薄膜可用作理想的 ETL。值得一提的是, 由于原位生长 SnO_2 方法无需添加具有强腐蚀性的盐酸和有毒的巯基乙酸, 未来亦可扩展应用于不耐腐蚀的 ITO 柔性透明导电衬底。

关 键 词: 钙钛矿太阳能电池; 共形氧化锡薄膜; 原位生长

中图分类号: TQ174 **文献标志码:** A **文章编号:** 1000-324X(2024)12-1397-07

Supporting information:

In-situ Growth of Conformal SnO_2 Layers for Efficient Perovskite Solar Cells

LIU Suolan[1,2], LUAN Fuyuan[1,3], WU Zihua[3,4], SHOU Chunhui[5], XIE Huaqing[3,4], YANG Songwang[1,2]

(1. CAS Key Laboratory of Materials for Energy Conversion, Shanghai Institute of Ceramics, Chinese Academy of Sciences, Shanghai 201899, China; 2. Center of Materials Science and Optoelectronics Engineering, University of Chinese Academy of Sciences, Beijing 100049, China; 3. School of Energy and Materials, Shanghai Polytechnic University, Shanghai 201209, China; 4. Shanghai Engineering Research Center of Advanced Thermal Functional Materials, Shanghai 201209, China; 5. Zhejiang Baima Lake Laboratory Co. Ltd., Hangzhou 310000, China)

Characterization

Scanning electron microscopy was performed using a Thermo Scientific G4 UC. The transmittance spectra were measured with a U-2800 UV-Vis spectrometer. Atomic force microscopy images were obtained using an NTEGRA instrument. A Yamashita Denso YSS-150A solar simulator was used to measure the PCE of the PSCs under one sun (100 $mW \cdot cm^{-2}$) and calibrated using a reference silicon photodiode with a BS-520BK filter (Bunkoukeiki, Japan). Steady-state photoluminescence spectra were characterized using a FluoroMax-4 steady-state fluorescence test system with an excitation wavelength of 532 nm. Electrochemical measurements were performed by a Zahner GIMPS electrochemical workstation (1 Hz–1 MHz). The dependence of V_{OC} on light intensity was investigated using an LED light source (LSW-2, 4300 K, 100 $mW \cdot cm^{-2}$). The incident photon-to-electron conversion efficiency spectra were measured by a Bunkoh-Keiki CEP-1500 instrument with a step length of 10 nm. For the transient photocurrent and transient photovoltage measurements, the record time of transient photocurrent and transient photovoltage was 10 ms, with a potentiostat setting time of 0.2 μs. During the 2 s light exposure, 10% of the data was captured before triggering, while 90% was captured after triggering. When recording the photovoltage decay process, the potentiostat was off-state. When recording the photocurrent decay process, it was necessary to turn on the potentiostat and apply a voltage of 0 V.

Table S1 Photovoltaic parameters of the perovskite solar cells

Sample	V_{OC}/V	J_{SC}/($mA \cdot m^{-2}$)	FF/%	PCE/%
SC SnO_2	1.0950±0.0165	24.910±0.156	73.650±1.278	20.080±0.376
IG SnO_2	1.1170±0.0126	25.060±0.079	76.650±0.809	21.450±0.321

Table S2 Fitting parameters of the TPC and TPV curves

Curve	Parameter	SC SnO_2	IG SnO_2
TPC	τ/μs	7.45	4.23
TPV	A_1	0.586	0.617
	τ_1/ms	0.232	0.094
	A_2	0.244	0.197
	τ_2/ms	1.548	1.539
	τ_{avg}/ms	1.199	1.307